Malaysian Journal of Civil Engineering 22(1) : 66-82 (2010)

FLOW FIELDS IN FRONT OF AN OBSTACLE

Bambang Yulistiyanto

Civil and Environmental Engineering Department, Faculty of Engineering
Gadjah Mada University, Jl. Grafika 2 Yogyakarta 55281

Corresponding author: *yulis@tsipil.ugm.ac.id*

Abstract : An experimental investigation, conducted in two different flows Reynolds number, was carried out to study the structure of the flow field upstream of a cylinder obstacle. An ADV Profiler was used to obtain instantaneously the three directions of the mean velocity in the stagnation plane. Results of the experiments show the longitudinal velocities, $\overline{u}$, decrease approaching the cylinder, their distribution becomes more uniform and close to the bed a reverse flow is noticeable with increasing importance. The downward velocity component is clearly shown, continuing with the return flow near the bed, forming a vortex. At positions where the vortex appears in the upstream from the cylinder, a large increase of the three components of the turbulence intensities is remarked. Approaching the cylinder, one observes the shear stress decreases, having the opposite direction at positions close to the cylinder. A zero value of shear stress should be at the separation point.

Keywords : *experimental investigation;, velocities distribution; horseshoe-vortex*

1.0 Introduction

A complex flow fields is established if flow is disturbed by a cylinder obstacle. The flow upstream will undergo a separation of the turbulent boundary layer and rolls up to form the well-known horseshoe-vortex system. This type of flow occurs in a variety of situations, such as flow around bridge piers, around buildings and structures, and at different types of junctions.

The experiments done with airflow over round and round-nosed objects have been investigated by numerous authors (see Baker, 1980, Eckerle and Langston, 1987, Pierce and Tree, 1990, Eckerle and Awad, 1991, Agui and Andreopoulos, 1992, Monti, 1994, Monnier and Stanislas, 1996) and with free surface flow (see Bolcs, 1969, *Dargahi*, 1987, *Magini*, 1993, Graf and Yulistiyanto, 1998). Similar experiment measurements were conducted by Abdul

Karim Barbhuiya and Subhasish Dey (2004), for flow around a vertical semicircular cylinder attached to the sidewall and at a wing-wall abutment installed at a rectangular channel, and by Andreas Roulund at.al. (2005).

This study investigates flow fields upstream a cylinder by using experiment data conducted in open channel (Yulistiyanto, B., 1997).

2.0 Research Method

Measurements of velocity and turbulence upstream an obstacle were conducted for two different flow Reynolds number. The velocity and turbulence profiles at some measuring station were measured by using the Acoustic Doppler Velocity Profiler (ADVP)-instrument during about 60 seconds and using the emission frequency of 1 MHz. Data analyses were then performed to get the velocity and turbulence profiles at different height of 4.65 [mm] intervals.

Cylindrical coordinates are used to denote the position of the measuring station in which P (r , α , z) and Q(r , α , z) refer to one of Test 1 and of Test 2, respectively. r is the distance from the center of cylinder to P or Q; α is equal to zero for upstream directions of an obstacle position. Ten measurement points were selected upstream from a cylinder, at distance varying from 12 cm to 44 cm. Smaller intervals were adopted for those close to the cylinder.

The friction velocities are calculated at first using the energy gradient, supposed equal to the bed slope for uniform flow, $S_f = S_o$, using $u_{*e} = \sqrt{ghS_f}$. Subsequently the Weisbach-Darcy coefficient, f, is calculated using $f = 8(u_{*e}/U)^2$. These calculated values are summarized in Table 1. The semi-empirical equation of Colebrook and White (see *Graf & Altinakar*, 1993, p.75) given by eq. 1, is then used to determine the uniform roughness, k_S:

$$\frac{1}{\sqrt{f}} = -2\log\left(\frac{k_s / R_h}{11.55} + \frac{3.86}{4\,\mathrm{Re}_h\sqrt{f}}\right) \tag{1}$$

The roughness Reynolds number, ($k_S u_{*e}/\nu$), can now be calculated (see Table 1). It can be concluded that the channel bed is in the transitional regime (see *Graf & Altinakar*, 1993).

Table 1 Uniform flow parameter and friction velocities.

Test	U [m/s]	u_{*e} [m/s]	f [-]	k_S [-]	$\frac{k_s u_{*e}}{\nu}$	u_{*r} [m/s]	u_{*cl} [m/s]	$\frac{u_{*cl}-u_{*r}}{u_{*r}}$	$\frac{u_{*e}-u_{*r}}{u_{*r}}$	B_{tr} [-]	Π [-]
1	0.67	0.034	0.0202	0.00043	14.5	0.029	0.0310	6.9%	17%	9.98	0.15
2	0.43	0.022	0.0206	0.00038	8.4	0.021	0.0207	-1.4%	4.7%	9.77	0.15

3.0 Results Of Measurements And Discussion

The measurements upstream from the cylinder for Test 1 and Test 2, $\alpha_1=\alpha_2=0°$, were taken at 10 or 11 different stations with the distance of the measurement from the center of the cylinder, *r*, in the range of 12.0 [cm] to 44.0 [cm], or r/D in the range of 0.5 to 2.

The tristatic ADVP-instrument performed the measurements from *P* (44.0, 0°, *z*) to *P* (15.0, 0°, *z*), and from *Q* (44.0, 0°, *z*) to *Q* (14.0, 0°, *z*), resulting in the three directions of the mean velocity profiles as well as their turbulence intensity and two components of the Reynolds stresses.

Measurements at *P* (14.0, 0°, *z*) to *P* (12.0, 0°, *z*), and at *Q* (13.0, 0°, *z*) to *Q* (12.0, 0°, *z*) were also done by the tristatic ADVP-instrument system in the *y-z* plane, giving results of the velocity profiles in the transversal, $\bar{v}$, and in the vertical, $\bar{w}$, directions and their turbulence intensity, $\sqrt{\overline{v'^2}}$ and $\sqrt{\overline{w'^2}}$; as well as results of the Reynolds stress in the transversal direction, $\overline{v'w'}$. Detail explanation of the tristatic ADVP-instrument is found elsewhere (Yulistiyanto, 1997). Results of these measurements are presented and discussed as the following.

3.1 Velocity profiles

Figures 1 and 2 show the profiles of the mean velocity along the symmetry plane upstream from the cylinder, adimensionalized by the approach velocity, U_∞, are plotted against the relative depth, *z/h*. Approaching the cylinder one observes (see Figs. 1 and Figs. 2.) the following: The longitudinal velocities, $\bar{u}$, decrease; their distribution becomes more uniform and close to the bed a reverse flow is noticeable with increasing importance. Profiles of measurements far from

the cylinder have the logarithmic distribution, whereas close to the cylinder, from P (15.0, 0°, *z*) to P (12.0, 0°, *z*) and from Q (15.0, 0°, *z*) to Q (12.0 , 0°, *z*), the shape of $\bar{u}(z)/U_\infty$ becomes more rectangular, and the maximum velocity is already reached far away under the water surface.

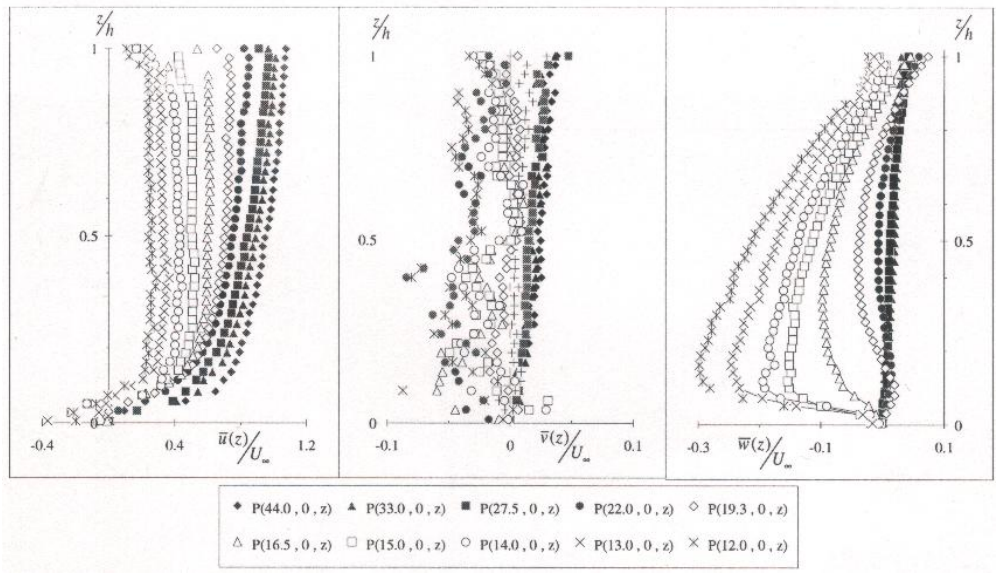

Figure 1 : Dimensionless velocities fo Test 1

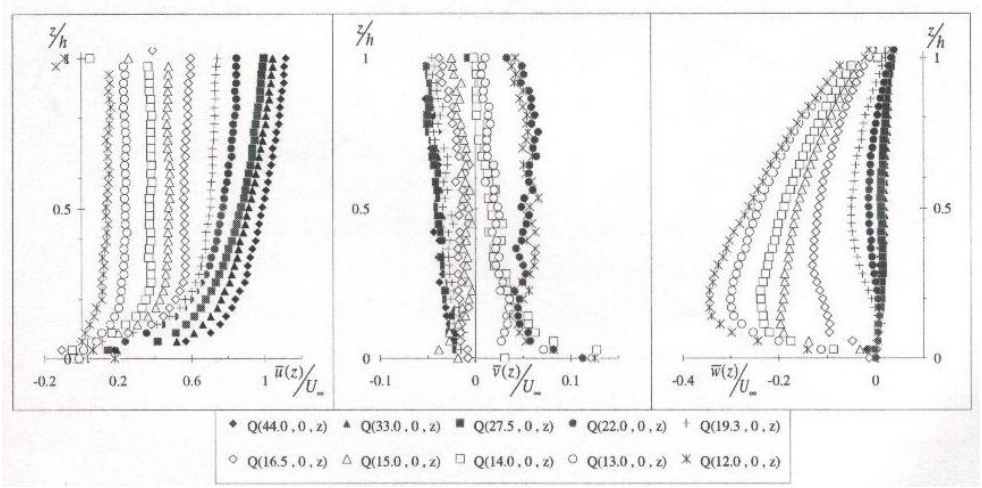

Figure 2 : Dimensionless velocities fo Test 2

The vertical (downward) velocity, $\overline{w}$, distributions at measurements far from the cylinder are small. Approaching the cylinder, their values increase and have a quasi triangular shape for measurements close to the cylinder, from P (15.0, 0°, *z*) to P (12.0, 0°, *z*) and from Q (16.5, 0°, *z*) to Q (14.0, 0°, *z*). Its distributions have a zero value at the surface and a maximum value near the bed. The downward velocity component increases while the longitudinal component decreases. The maximum downward flow is about $\overline{w} = 0.3U_{\infty}$ at P (12.0, 0°, *z*) for Test 1, and $\overline{w} = 0.35U_{\infty}$ at Q (12.0, 0°, *z*) for Test 2. These are smaller values than those presented by *Ettema* (1980). Ettema's measurement at 0.02 - 0.05 *D* from the cylinder wall, where *D* is the diameter of the cylinder, gave a maximum value of $\overline{w} = 0.4\ U_{\infty}$, near the bed.

The mean transversal, $\overline{v}$, velocity is uniform over the depth and is much smaller compared to the longitudinal and the vertical ones and no conclusion can be deduced to indicate the effect of the cylinder.

Figure 3 and Figure 4 show the velocity vectors of the bidimensional velocities, $\overline{u}_r$ and $\overline{w}$, for Test 1 and Test 2, respectively. The $\overline{u}_r$, equivalent to the negative longitudinal velocity, $-\overline{u}$, decreases as it approaches the cylinder. The downward flow near the edge of the cylinder is clearly shown, continuing with the return flow near the bed, forming a vortex. The position of the separation point, S_V, could not be exactly defined from this velocity vector, due to the small measurement density in the radial direction. However, this position can be presumed to be between the last positive velocity and the next negative (reverse) velocity at the bed, which lies between *r* = 19.5[cm] and *r* = 16.5 [cm] for both tests.

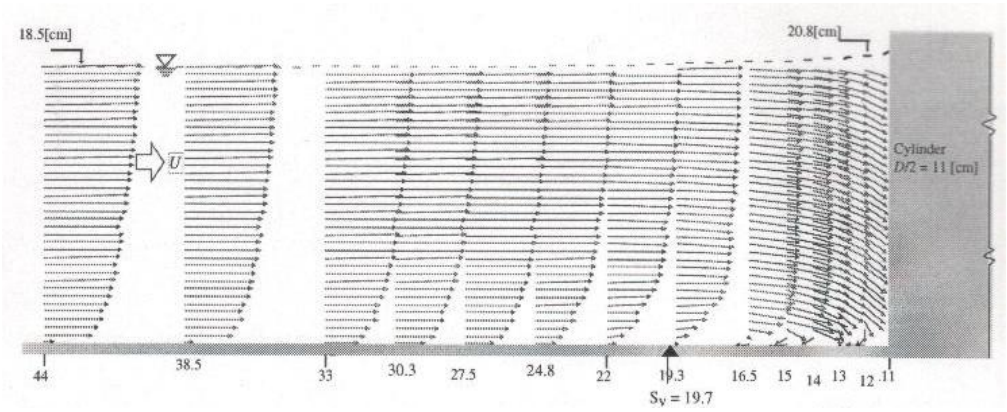

Figue 3 : Velocity vectors for Test 1

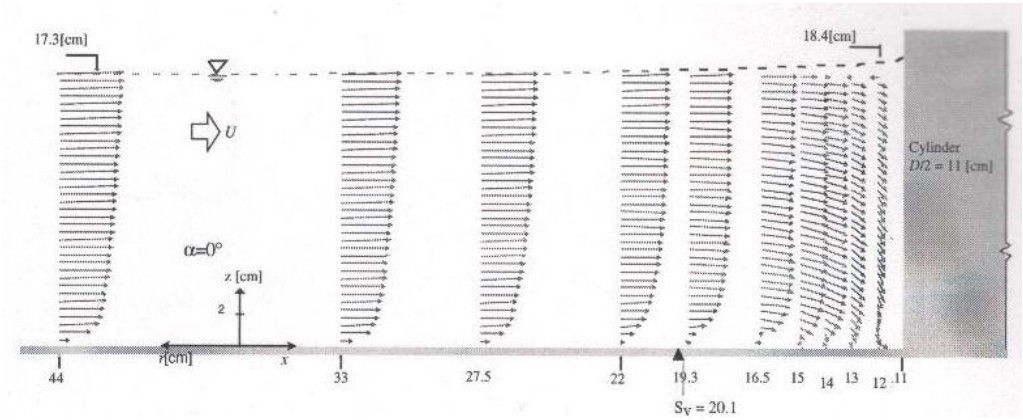

Figure 4 : velocity vectors for Test 2

The longitudinal velocity profiles for Test 1, plotted as $\frac{\bar{u}(z)}{u_{*cl}}$ against $\frac{u_{*cl}z}{\nu}$, are presented in Figure 5, for Test 2, they are found elsewhere (Yulistiyanto B., 1997). In open channel flow two regions can be distinguished, the inner and outer regions. Velocity distributions within the inner region, $z/h < 0.2$, for transitional regime can be expressed by the universal law of the wall, the log-law, as:

$$\frac{\bar{u}(z)}{u_{*cl}} = \frac{1}{\kappa}\ln\left(\frac{z}{k_s}\right) + B_{tr} \qquad (2)$$

$$B_{tr} = 8.5 + \left[2.5\cdot\ln\left(\frac{u_{*c}k_s}{\nu}\right) - 3\right]\cdot e^{-0.217\left[\ln\left(\frac{u_{*c}k_s}{\nu}\right)\right]^2}$$

where $\bar{u}(z)$ is the mean-local velocity at a distance, z, measured from the bed; $\kappa = 0.4$ is the Karman's universal constant; u_{*cl} is the friction velocity; ν is the molecular viscosity; and B_{tr} is the numerical constant of integration.

The measured data are then evaluated using this logarithmic velocity distribution, equation 2. This allows to calculate the friction velocity, u_{*cl} (according to Clauser), and the constant of integration, B_{tr}, by trial and error.

These values are summarized in Table 2. The found numerical constant of integration, B_{tr}, is in agreement with the ones in the literature. It is shown in Figure 5, that the profiles in the inner region coincide quite well with the log-law, eq. 2, except for points near the bed. These unexpected points are due to a part of the measurement volumes that are under the mylar (see *Yulistiyanto B., 1997)*). However measurements close to the cylinder, from Q (15.0, 0°, *z*) to Q (12.0 , 0°, *z*), some points near the bed fall below the logarithmic line. These may be influenced by the presence of the vortex.

The velocity distribution in the outer region, *z/h* > 0.2, deviates from the log-law, as shown in Figure 5. Coles (1956) developed a formula for this region as follows:

$$\frac{\bar{u}(z)}{u_{*cl}} = \frac{1}{\kappa}\ln\left(\frac{z}{k_s}\right) + B_{tr} + \frac{2\Pi}{\kappa}\sin^2\left(\frac{\pi z}{2h}\right) \tag{3}$$

where *h* is the water depth; Π is the wake strength parameter. In eq. 3, all values are known and the wake strength parameter, Π, can be determined; they are listed in Table 2.

The data in the outer region, *z/h* > 0.2, are evaluated using the Coles's method, by introducing the value of the wake-strength, Π. The observations show that the data are coincided well with the Coles's line, excepting some points near the surface for measurements close to the cylinder that fall under the line. The summary of the found friction velocity, the constant of integration, and the wake strength is presented in.

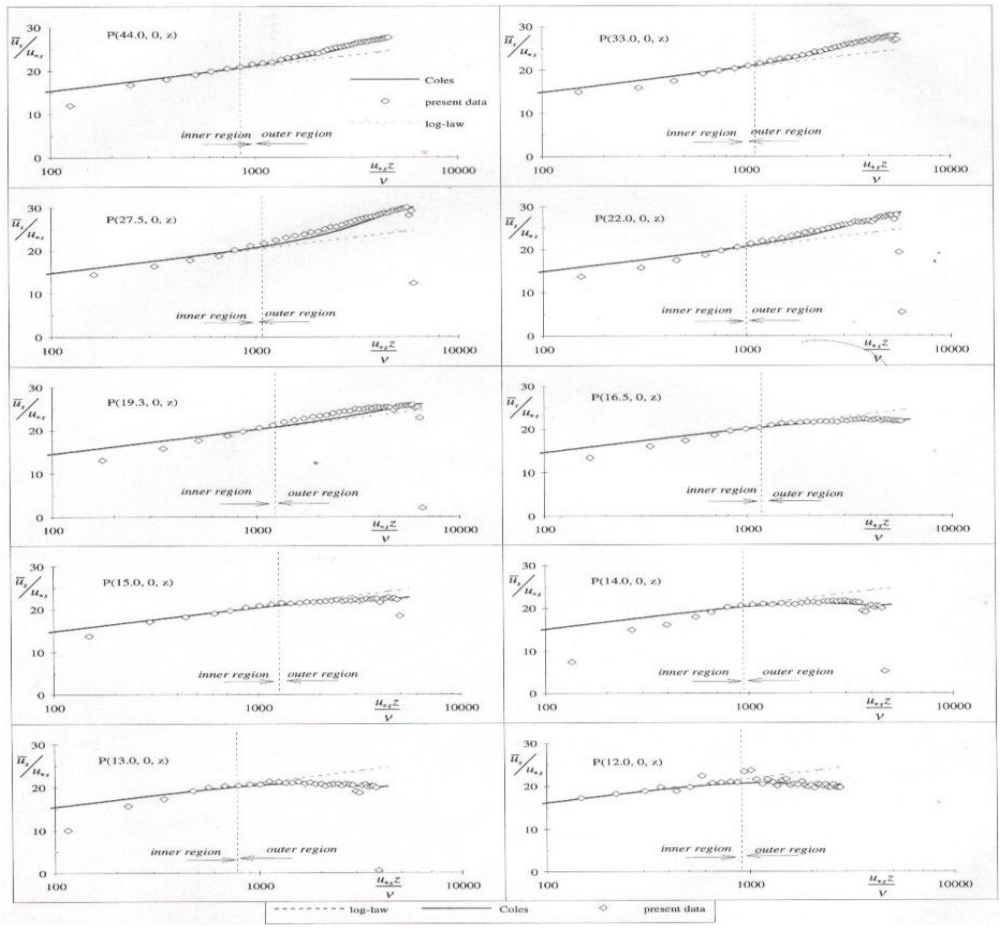

Figure 5: The longitudinal velocity profiles for Test 1

Table 2 : The found friction velocity, the constant of integration, and the wake strength

Position	u_*	B_{tr}	Π
P(44.0,0,*z*)	0.0260	9.949	0.60
P(33.0,0,*z*)	0.0315	9.984	0.75
P(27.5,0,*z*)	0.0335	9.986	1.10
P(22.0,0,*z*)	0.0320	9.985	0.80
P(19.3,0,*z*)	0.0365	9.982	0.30
P(16.5,0,*z*)	0.0350	9.985	-0.5
P(15.0,0,*z*)	0.0310	9.983	-0.4
P(14.0,0,*z*)	0.0280	9.968	-0.8
P(13.0,0,*z*)	0.0240	9.920	-0.9
P(12.0,0,*z*)	0.0155	9.607	-0.8

3.2 Turbulence intensity profiles

The Root Mean Square (RMS) values of the velocity fluctuations of flow, $\sqrt{\overline{u'^2}}$, $\sqrt{\overline{v'^2}}$, and $\sqrt{\overline{w'^2}}$, upstream from the cylinder measured by the tristatic ADVP-instrument are presented in Figs. 6 for Test 2. Results for Test 1 are rather similar.

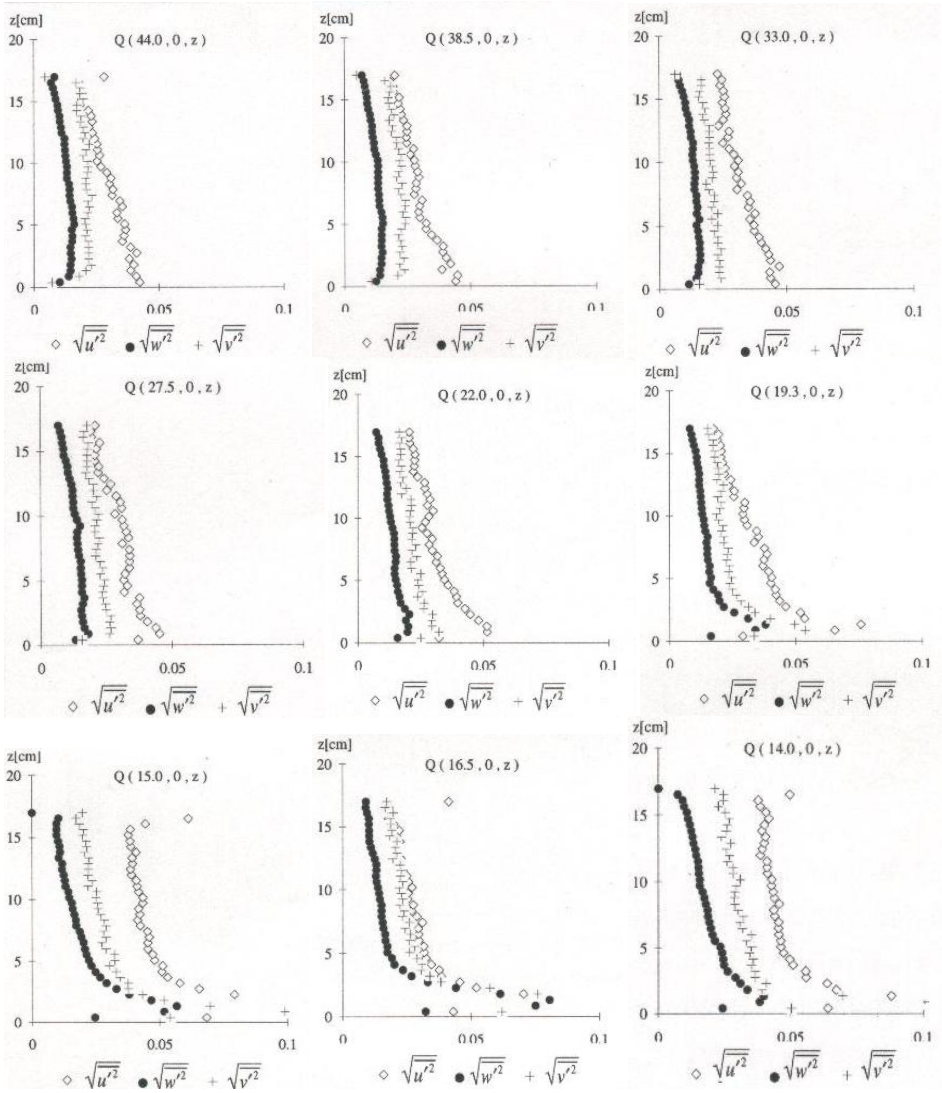

Figure 6 : Turbulence intensities for Test 2

The profiles show that the horizontal turbulence intensity, $\sqrt{\overline{u'^2}}$, decreases with the increase of *z* and reaches its minimum value near the water surface. At positions where the vortex appears, from Q(19.3 , 0°, *z*) to Q(14.0 , 0°, *z*) and near the bed, a large increase of the turbulence intensities is remarked. From Q(13.0 , 0°, *z*) to Q(12.0 , 0°, *z*), the horizontal turbulence intensities were not measured due to the limited space for the tristatic ADVP-instrument.

The vertical turbulence intensities, $\sqrt{\overline{w'^2}}$, have a minimum value at the surface. They increase with the depth, reaching maximum values at a certain level above the bed, then they decrease towards the bed. At positions where the vortex appears, from Q(19.3 , 0°, *z*) to Q(14.0 , 0°, *z*), the vertical turbulence intensity presents a significant peak in the lower region of the water depth, $z/h < 0.2$.

Far from the cylinder, the transversal turbulence intensities, $\sqrt{\overline{v'^2}}$, have rather uniform values from the water surface to near the bed, and decrease towards the bed. Measurements from Q(22.0, 0°, *z*) to positions closer to the cylinder, the $\sqrt{\overline{v'^2}}$ -profile decreases with increasing *z*, and has a similar tendency with those of the longitudinal and vertical turbulence intensity. Their values are always between the values of the longitudinal and vertical turbulence intensity.

Approaching the cylinder, the tendencies of the three components of the turbulence intensities, $\sqrt{\overline{u'^2}}$, $\sqrt{\overline{v'^2}}$ and $\sqrt{\overline{w'^2}}$, are similar; the profiles increase; this is very noticeable at some points near the bed.

The turbulence intensities are also presented as contours of the dimensionless turbulence intensities, $\sqrt{\overline{u'^2}}/U_\infty$, $\sqrt{\overline{v'^2}}/U_\infty$ and $\sqrt{\overline{w'^2}}/U_\infty$, as shown in Figs.7, which indicate regions close to the leading edge of the cylinder, where the turbulence intensities show sharp peaks. In front of the cylinder, the positions of the maximum turbulence intensities are in the regions of the horse-shoe vortex.

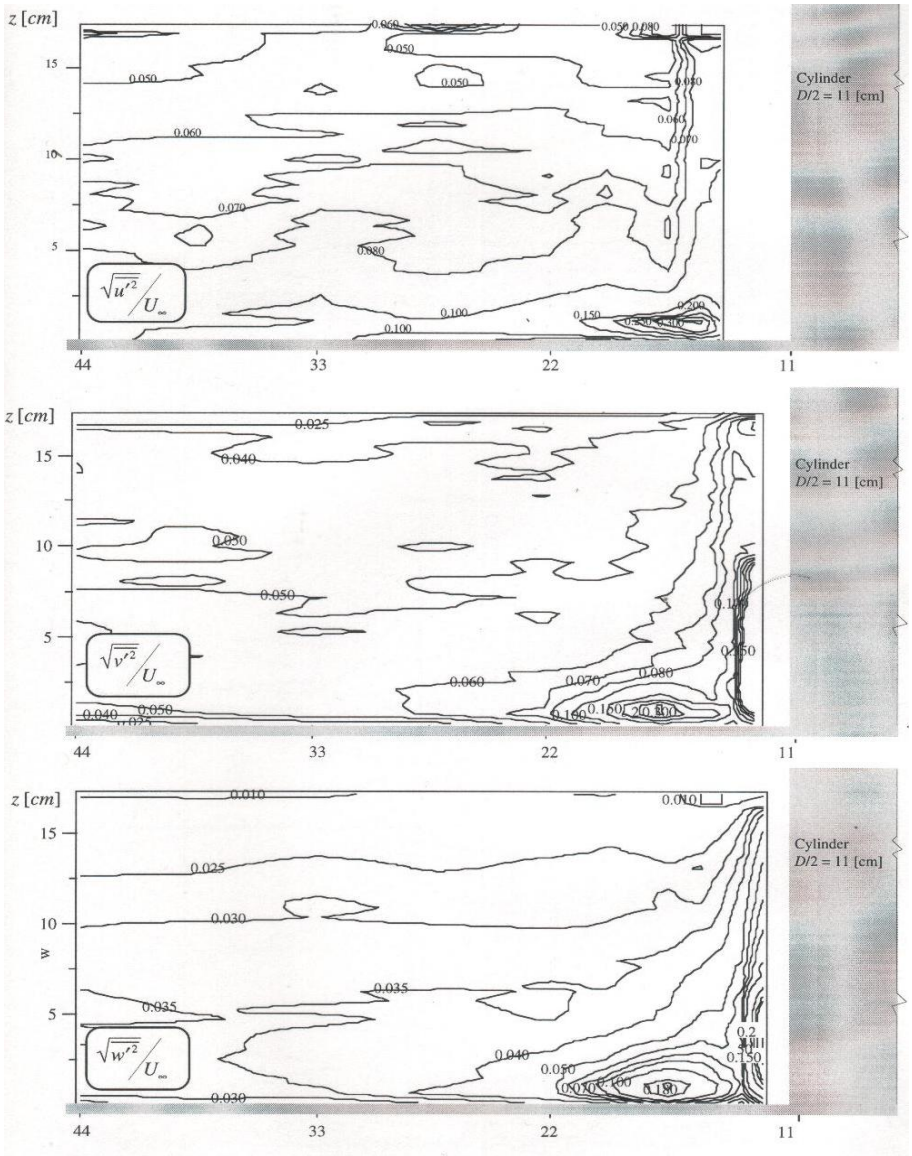

Figure 7 : Contours of the dimensionless turbulence intensities, Test 2

The turbulent kinetic energy (k) in the radial planes was calculated, using the following definition:

$$k = \frac{1}{2}\left(\overline{u'^2} + \overline{v'^2} + \overline{w'^2}\right) \tag{4}$$

The contours of the turbulent kinetic energy are presented in Figs. 8 and 9 for Test 1 and Test 2, respectively. Close to the cylinder there are regions where one composant of the turbulence was not measured, and are thus not shown. From these figures, one observes the maximum turbulence kinetic energy, $k^{\max}$, and its positions as the following:

Test 1: $k^{\max}$ = 0.025 [m^2/s^2] at (r/D = 0.72 ; z/D = 0.06)

Test 2: $k^{\max}$ = 0.020 [m^2/s^2] at (r/D = 0.73 ; z/D = 0.04)

The positions of the $k^{\max}$ as well as the maximum turbulence intensity, are in the regions of the vortices, a small vortex in the upstream from the cylinder.

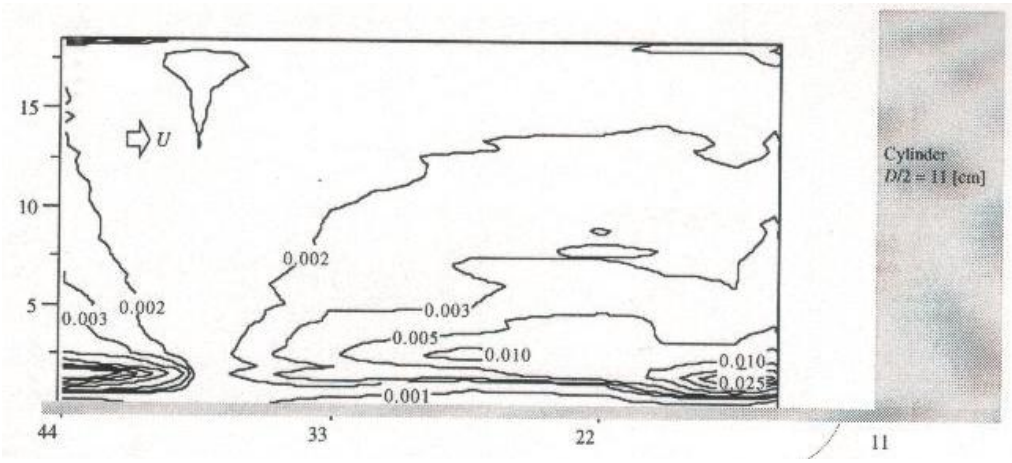

Figure 8 : Contours of the turbulent kinetic energy, Test 1

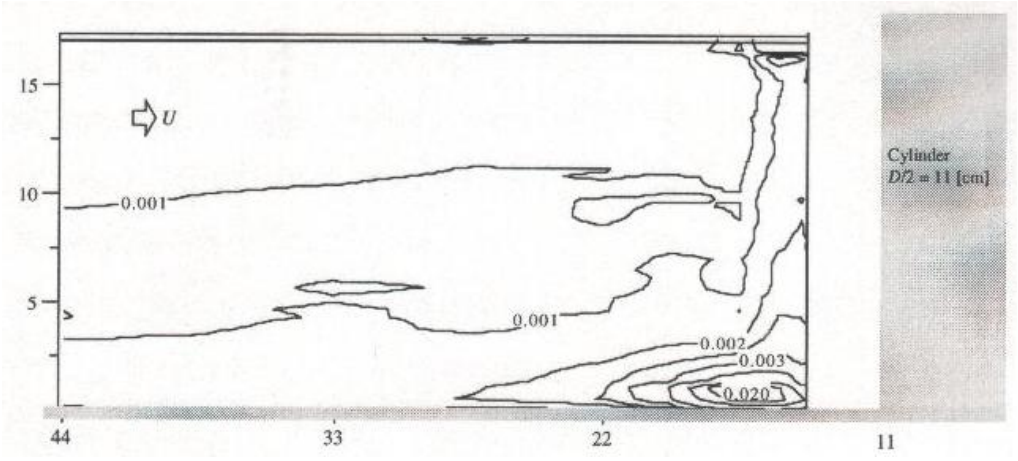

Figure 9 : Contours of the turbulent kinetic energy, Test 2

3.3 Reynolds stress profiles

In Figures 10, are plotted the measured Reynolds-stress profiles in two directions, $\overline{u'w'}$ and $\overline{v'w'}$, for Test 2. Applying the fitting to the measured data near the bed, we obtain the values of the friction velocities, u_{*_x} and u_{*_y}, at $z = 0$.

From Q(44.0, 0°, z) to Q(27.5, 0°, z), the Reynolds stress distributions have a maximum value at a certain distance close to the bed, and diminish towards a zero value at the water surface. Measurements from Q(22.0 , 0°, z) to Q(14.0 , 0°, z), present a significant peak at a certain level above the bed. The fitting of the data under this peak gives a negative value of the friction velocity from Q(19.3 , 0°, z) to Q(14.0 , 0°, z). From Q(13.0 , 0°, z) to Q(12.0 , 0°, z), the $\overline{u'w'}$ -profiles were not measured.

The $\overline{v'w'}$ values far upstream from the cylinder are small and have no well defined shapes. Measurements from Q(22.0 , 0°, z) to Q(14.0 , 0°, z), they have small values at the upper region of the water depth and increase towards the bed. At measurements close to the cylinder, from Q(13.0 , 0°, z) to Q(12.0 , 0°, z), the $\overline{v'w'}$ distributions have a triangular form with the maximum value near the bed then decrease monotonously towards both the water surface and the bed.

Approaching the cylinder, one observes the shear stress decreases, having the opposite direction at positions close to the cylinder. A zero value of shear stress should be at the separation point.

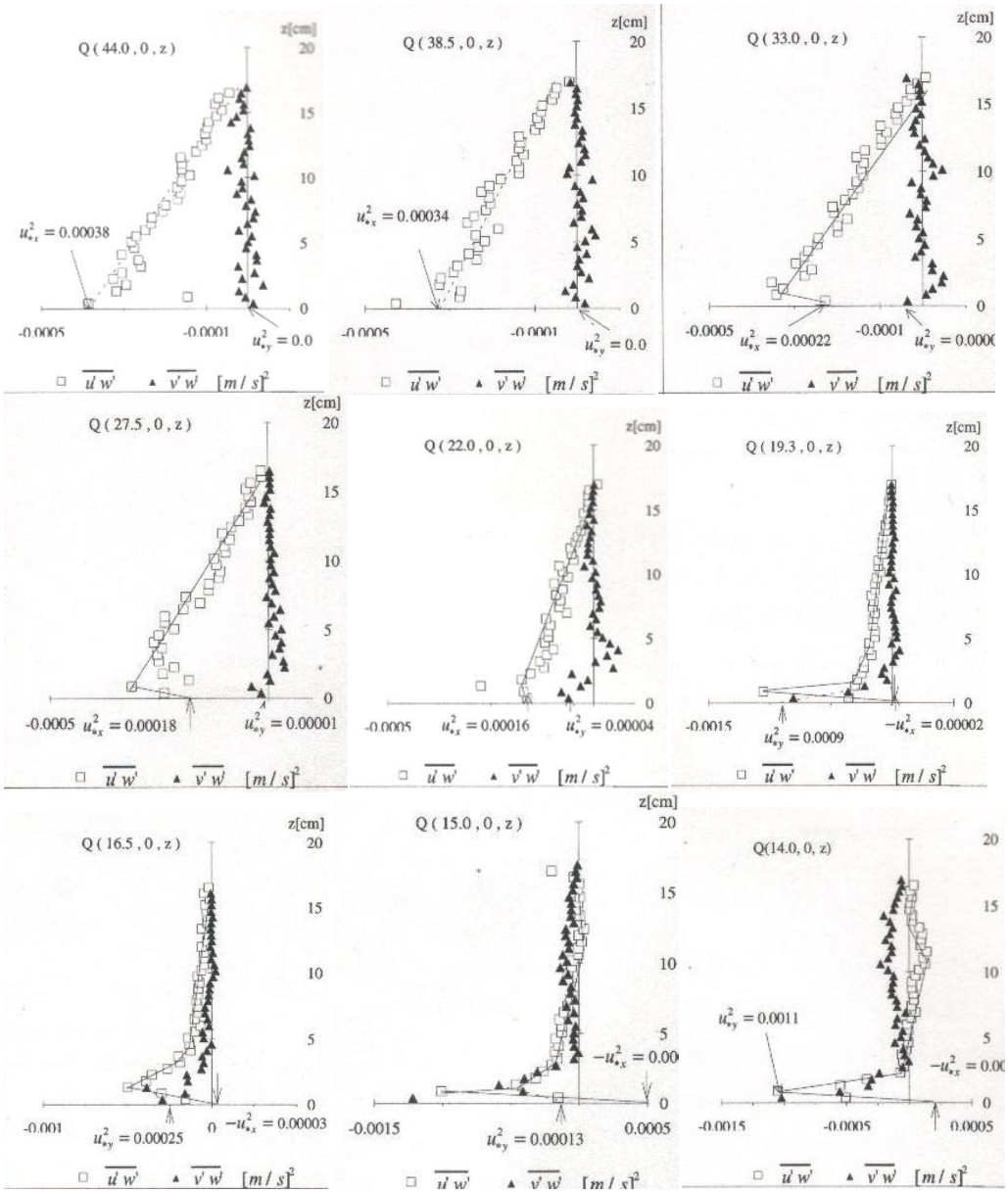

Figure 10 : Distributions of Reynolds Stresses for Test 2.

4.0 CONCLUSIONS

Based on the experiment results discussed in this paper, some findings are summaries in Figure 11, as:

- Measurements of the velocity and its turbulence intensities, upstream from a cylinder are reported for fully developed turbulent open-channel flow at $Re_D \approx 10^5$. This flow has been documented with the mean point velocity field. The measurements were made with a non-intrusive ADVP-instrument.
- Approaching the cylinder, the longitudinal velocities, $\overline{u}$, decrease; their distribution becomes more uniform and close to the bed a reverse flow is noticeable with increasing importance. The downward velocity component increases, reach $\overline{w}$ = 0.3- 0.35U_∞, This is clearly shown, continuing with the return flow near the bed, forming a vortex.
- At positions where the vortex appears in the upstream from the cylinder, a large increase of the three components of the turbulence intensities is remarked.
- Approaching the cylinder, one observes the shear stress decreases, having the opposite direction at positions close to the cylinder. A zero value of shear stress should be at the separation point.

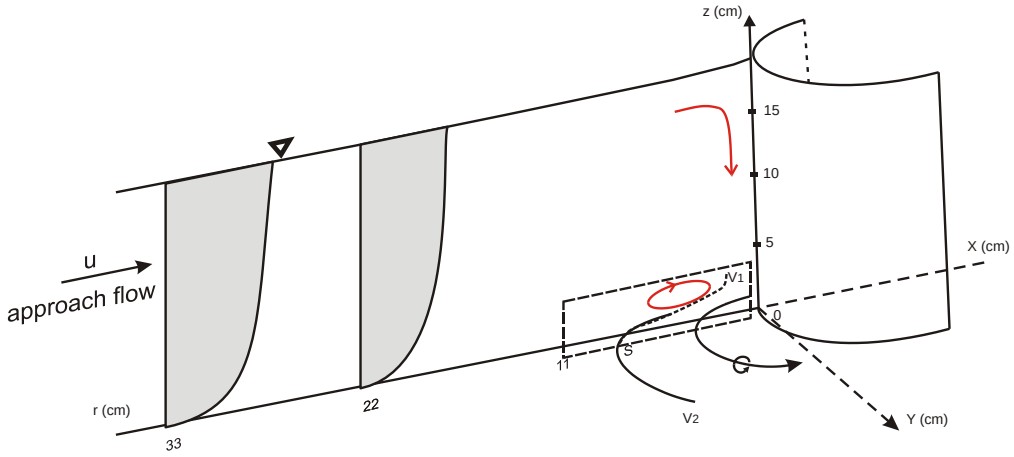

Figure 11 : Scheme of the Flow Fields Upstream of the Cylinder

References

Abdul Karim Barbhuiya and Subhasish Dey, Measurement of turbulent flow field at a vertical semicircular cylinder attached to the sidewall of a rectangular channel, *Flow Measurement and Instrumentation, Volume 15, Issue 2*, April 2004, Pages 87-96, Elsevier.

Abdul Karim Barbhuiya and Subhasish Dey, Velocity and turbulence at a wing-wall abutment, Sadhana Vol. 29, Part 1, February 2004, pp. 35–56, India.

Agui J.H. and Andreopoulos J.: " Experimental investigation of a three-dimensional boundary layer flow in the vicinity of an uprigth wall mounted cylinder", J. Fluids Engineering, Vol. 114, 1992, pp. 566-576.

Andreas R, B. Mutlu Sumer, F. Jorgen and M. Jess, Numerical and experimental investigation of flow and scour around a circular pile, Journal of Fluid Mechanics, 534:351-401, Cambridge, 2005.

Eckerle W.A. and Awad J.K.: " Effect of freestream velocity on the three-dimensional separated flow region in front of a cylinder", J. Fluids Engineering, Vol. 113, 1991, pp. 37-44.

Eckerle et Langston: " Horseshoe vortex formation around a cylinder", ASME J. of Turbomachinery, Vol. 109, April 1987, pp. 278-285.

Graf W.H. & M.S. Altinakar: Hydraulique fluviale; Tome 1, Presses Poly. et Univ. Romandes, Lausanne, CH, 1993.

Graf W.H. and B. Yulistiyanto: "Experiments on Flow around a cylinder; the velocity and vorticity fields", ", J. Hydraulic Research, Vol. 36, 1998, pp. 637-653.

Monnier J.C. and Stanislas M.: " Study of a horseshoe vortex by LDV and PIV", ERCOFTAC Bulletin, No. 30, 1996, pp. 19-24.

Pierce F.J. and I.K. Tree: " The mean flow structure and the symmetry plane of a turbulent junction vortex.", J. Fluids Engineering, Vol. 112, 1990, pp. 16-22.

Yulistiyanto B., Y. Zech and W.H. Graf: "Free-Surface Flow Around a Cylinder : Shallow-Water Modeling with Diffusion-Dispersion", Journal of Hydraulic Engineering, vol. 124 (no.4), 1997, pp. 419-429.

Yulistiyanto B. , Flow around a cylinder installed in a fixed-bed open channel, PhD dissertation 1631, Ecole Polytechnique federale, Lausanne, Switzerland, 1997.